


Combined 3D-QSAR, Molecular Docking, Binding Free Energy, and ADMET Profiling of Novel Substituted Pyrazolyl-Pyrimidinones as Potential Anti-HIV Agents

Badr Hamdache ^{1,*} , Kamal Tabti ^{2,*}, Sara Zarougui ³, Kacem Marieme ⁴, Mustapha Dib ⁴, Khadija Ouchetto ¹, Abdelouahid Sbai ², Menana Elhalaoui ³, Hajiba Ouchetto ¹

¹ Laboratory of Molecular Chemistry, Materials and Catalysis, Faculty of Science and Technology, Sultan Moulay Slimane University, BP 523, Beni-Mellal 23000, Morocco

² Molecular and Computational Chemistry, NSMC Laboratory, Faculty of Science, Moulay Ismail University of Meknes, Morocco

³ LIMAS Laboratory, Faculty of Sciences, Dhar El Mahraz, Sidi Mohamed Ben Abdellah University, Fez, Morocco

⁴ Laboratory of Applied Chemistry and Environment, Mineral Solid Chemistry Team, Faculty of Sciences, Mohammed First University, B.P. 717, 60 000, Oujda, Morocco

* Correspondence: k.tabti@edu.umi.ac.ma (K.T.); badrhamdache17@gmail.com (B.H.);

Received: 28.07.2024; Accepted: 11.04.2025; Published: 20.12.2025

Abstract: Non-nucleoside reverse transcriptase inhibitors (NRTIs) play a very important role in the treatment of HIV, among which the inhibitor (S-DABOs) stops the enzyme from transcribing HIV-1. In this study, we combined QSAR-3D modeling, molecular docking, and ADMET analyses for a series of 2-alkylsulfanyl-6-benzyl-3,4-dihydropyrimidine-4(3H)-ones. The QSAR-3D model is based on CoMFA and CoMSIA, which relate physicochemical descriptors to anti-HIV activity. The statistical criteria obtained from CoMFA are $q^2 = 0.532$ and $R^2 = 0.828$, and from COMSIA $q^2 = 0.721$ and $R^2 = 0.833$. The reliability and predictability capacity of the model are verified by the Golbraikh-Tropsha criteria. Except for the N18 compound, all molecules belong to the applicability domain range, and both models are satisfied for the prediction of the new antiviral compounds. The molecular docking results for the six proposed compounds indicate better stability and stronger ligand-protein interactions. The ADMET results for all predicted Compounds indicate good pharmacokinetic properties and non-toxicity. According to these data, the prediction compounds present good anti-HIV candidates.

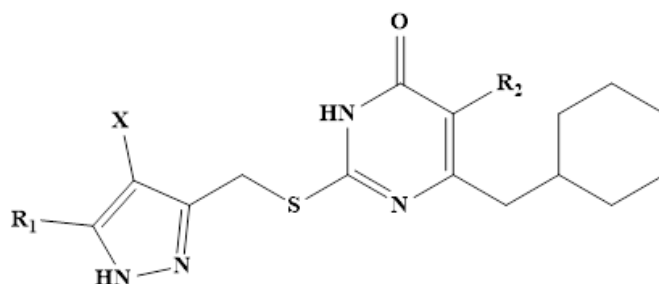
Keywords: 3D-QSAR; molecular docking; anti-HIV activity; bioactive molecules; pyrazolyl-pyrimidinones; MD simulation; and ADMET profiling.

© 2025 by the authors. This article is an open-access article distributed under the terms and conditions of the Creative Commons Attribution (CC BY) license (<https://creativecommons.org/licenses/by/4.0/>), which permits unrestricted use, distribution, and reproduction in any medium, provided the original work is properly cited. The authors retain copyright of their work, and no permission is required from the authors or the publisher to reuse or distribute this article, as long as proper attribution is given to the original source.

1. Introduction

AIDS (Acquired Immunodeficiency Syndrome) is a disease caused by HIV-1 infection (Human Immunodeficiency Virus Type 1). HIV-1 attacks the immune system, specifically CD4 cells (T lymphocytes) [1], which are essential to the body's ability to fight infections. As HIV-1 progresses, it weakens the immune system, making the body more susceptible to opportunistic infections and certain types of cancer. If untreated, HIV-1 infection can lead to AIDS, which is characterized by severe immunodeficiency and the presence of one or more opportunistic infections or diseases defined by AIDS [2]. Non-nucleoside reverse transcriptase inhibitors (NNRTI NRTIs) are an important class of antiretroviral drugs used in the treatment

of HIV-1. They act against reverse transcriptase, a key enzyme that HIV-1 uses to replicate. NNRTI INTIs bind to reverse transcriptase and prevent the virus from converting its viral RNA to viral DNA, thereby disrupting the HIV-1 replication cycle [3]. Some examples of NNRTI INTIs include efavirenz, nevirapine, and etravirine. These drugs are important components of many combined antiretroviral therapies for HIV-1 [4]. According to statistics carried out by UNAIDS institutes and other health organizations, it is estimated that by 2022, about 38 million people in the world will be living with HIV. New infections, about 1.5 million new HIV infections are registered each year, and about 680,000 [5]. AIDS-related deaths are recorded every year, since acquired immunodeficiency syndrome (AIDS) is the most devastating pandemic. The high resistance and rapid mutation rates of the virus-VIH render existing NNRTI drugs ineffective, prompting the discovery of new NNRTI drugs with good biological activity [6,7]. Bioactive nitrogen-containing heterocyclic molecules play an essential role in organic chemistry and pharmaceutical chemistry thanks to their importance and significant therapeutic potential [7-13]. The heterocyclic compounds that contain S and N are most biologically active, such as the anti-HIV activity [13-15]. It has also been noted that SDABOS derivatives are non-nucleosidic HIV reverse transcriptase (NNRTI) inhibitors for wild viruses [14]. 2-alkylsulfanyl-6-benzyl-3,4-dihydropyrimidine-4(3H)-ones (S-DABOs) derivatives contain biologically attractive N-nitrogen clusters, cry donor hydrogen-bonding [15,16], and amino acid residues of target proteins [18] that are recognized by reverse transcriptase (RT) during the HIV-1 lifecycle, making them among the most widely used NNRTIs in the pharmaceutical field. S-DABOs compounds due to their biological antiviral activity and low toxicity [19,20]. A modification on SDABOS allows the identification of a series of 40 molecules of new substituted 2-(5-alkyl/aryl-1H-pyrazole-3-yl)me-thyl(thio)-5-alkyl-6-(cyclohexylmethyl)-pyrimidin-4(3H) scheme 1, one with excellent antiviral effect against HIV-1 [21,22]. Therefore, the prediction of new HIV drugs by computer-assisted techniques is now implicit in decreasing the cost and time of developing highly efficient and specific drugs [23]. Using the three-dimensional quantitative relationship structure-activity (3D-QSAR) to establish a mathematical relationship structure for biological activity, molecular docking, ADMET are essential to understanding the types of interactions between the drug and the active site of the protein, water solubility, toxicity, and stability of each ligand to identify a good, reliable model in order to obtain new antiviral medications [24,25,26]. The design of new antiviral compounds by the structure-activity method (QSAR) [27]. The 3D-QSAR study is carried out using the comparative analysis of molecular fields with indices (CoMFA and CoMSIA) [28,29]. To validate the reliability of the CoMFA and CoMSIA models based on internal validation and external validation [30,31]. In this study, we proposed new anti-HIV compounds using 3D-QSAR, molecular docking, MD simulation, and ADMET profiling [32,33].



Scheme 1. Chemical structure of pyrazolyl-pyrimidinone derivatives.

2. Materials and methods

2.1. Database.

In this work, we have a dataset of 40 molecules (NNRTIs) from the pyrazole and pyrimidine families, published in reference [34], with experimental EC50 values converted to $pEC_{50} = -\log(EC_{50})$, as shown in Table 1. These values range from 8.420 to 11, with 4.5 as the minimum compound value, 40 for drawing and optimization, and backed up again to the mol2 format of these molecules using ChemDraw 8.0. The study of these molecules is carried out manually and divided into two groups: a training set of 32 compounds (80%) to generate the QSAR-3D model, and a test set of 8 molecules (20%) to validate the robust model.

Table 1. Activities against the anti-VIH of pyrazolyl-pyrimidinones derivatives.

Compound	R1	R2	X	pEC50	CoMFA	Residus	CoMSIA	Residus
1	Ph	Et	H	8.16	7.702	0.458	7.724	0.436
2*	3'-Me-Ph	Et	H	7.131	7.345	-0.214	7.402	-0.271
3*	3'-Br-Ph	Et	H	7.290	7.054	0.236	7.034	0.256
4*	3'-Cl-Ph	Et	H	7.177	6.988	0.189	7.221	-0.044
5	3'-F-Ph	Et	H	7.458	7.519	-0.061	7.454	0.004
6*	3'-CF3-Ph	Et	H	6.521	6.961	-0.44	7.052	-0.531
7	4'-Me-Ph	Et	H	7.282	7.083	0.199	7.246	0.036
8	4'-Cl-Ph	Et	H	7.750	7.382	0.368	7.143	0.607
9*	4'-F-Ph	Et	H	7.699	7.442	0.257	7.522	0.177
10	4'-MeO-Ph	Et	H	7.635	7.779	-0.144	7.739	-0.104
11	4'-OH-Ph	Et	H	8.420	7.692	0.728	8.412	0.008
12	4'-MeS-Ph	Et	H	7.928	7.883	0.045	7.770	0.158
13	4'-(CH3)2CH-Ph	Et	H	6.833	6.839	-0.006	6.790	0.043
14	3',4'-diCl-Ph	Et	H	6.508	6.645	-0.137	6.695	-0.187
15	3',4'-diF-Ph	Et	H	6.791	7.153	-0.362	6.951	-0.16
16	2',4'-diMe-Ph	Et	H	6.322	6.857	-0.535	6.767	-0.445
17	2',4'-diF-Ph	Et	H	7.370	7.408	-0.038	7.185	0.185
18	2'-N-pyridyl	Et	H	7.642	7.436	0.206	7.608	0.034
19	H	Et	H	7.476	7.528	-0.052	7.640	-0.164
20*	Me	Et	H	7.558	7.583	-0.025	7.864	-0.306
21	Cyclopropyl	Et	H	7.611	7.652	-0.041	7.534	0.077
22	C(CH3)3	Et	Cl	6.528	6.545	-0.017	6.484	0.044
23	Ph	Et	Cl	7.004	7.448	-0.444	7.456	-0.452
24	3'-Me-Ph	Et	Cl	7.066	7.448	-0.382	7.148	-0.082
25*	3'-Br-Ph	Et	Cl	6.994	7.049	-0.055	7.069	-0.075
26	3'-Cl-Ph	Et	Cl	7.24	6.752	0.488	7.011	0.229
27	3'-F-Ph	Et	Cl	7.147	7.311	-0.164	7.289	-0.142
28	3'-CF3-Ph	Et	Cl	6.740	6.680	0.06	6.594	0.146
29	4'-Me-Ph	Et	Cl	6.860	6.996	-0.136	6.994	-0.134
30	4'-Cl-Ph	Et	Cl	7.049	7.176	-0.127	6.893	0.156
31	4'-F-Ph	Et	Cl	7.742	7.242	0.500	7.259	0.483
32	3',4'-diCl-Ph	Et	Cl	6.457	6.397	0.06	6.419	0.038
33	3',4'-diF-Ph	Et	Cl	6.820	7.047	-0.227	7.095	-0.275
34	4'-MeO-3'-Cl-Ph	Et	Cl	6.886	6.876	0.010	6.973	-0.087
35	Ph	CH3	H	6.729	6.865	-0.136	6.634	0.095
36*	4'-MeO-Ph	CH3	H	6.712	6.968	-0.256	6.499	0.213
37	4'-F-Ph	CH3	H	6.449	6.369	0.08	6.447	0.002
38	Ph	H	H	5.303	5.312	-0.009	5.313	-0.01
39	4'-MeO-Ph	H	H	5.403	5.395	0.008	5.262	0.141
40	4'-F-Ph	H	H	4.997	4.943	0.054	9.334	-4.337

*Test set

2.2. Database minimization and alignment.

QSAR-3D studies of 40 pyrimidine parasol molecules using SYBYL.X2.0 software initially minimize the energy of 40 molecules, employing the standard Tripos Field Force, which uses the Gasteiger-Huckel method to add partial atomic charges [35,36], the molecular minimize studied by fixed gradient finish characteristics of 0.01 kcal/mol, the maximum number of 1000 iterations with Dielectric of the constant distance of 1.00, and the NB Cutoff of 8.00. Subsequently, it performs alignment of the molecular structures studied in 3D space according to their associated orientations. This is a more important step in the QSAR-3D study to develop a robust predictive model using CoMFA and CoMSIA [37]. In this study, the alignment of molecules in the database was achieved using the distillation method, with substance 11, an excellent anti-HIV agent, as the model molecule. All the remaining 39 molecules are aligned with the common structure of compound 11. Figure 1 shows the aligned molecules.

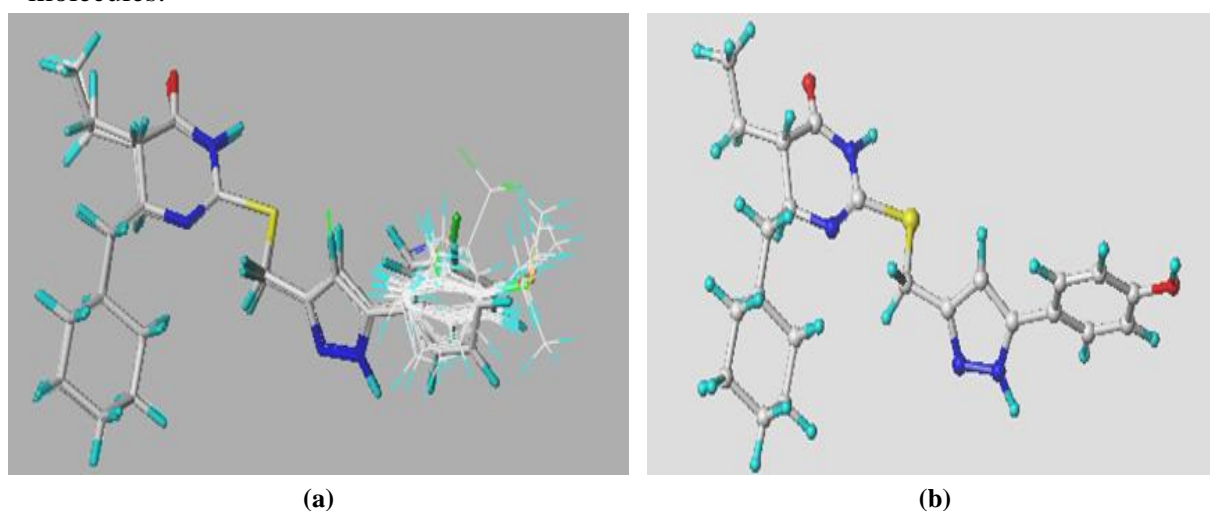


Figure 1. (a) All 40 molecules align; (b) base molecule.

2.3. Model construction QSAR-3D.

2.3.1. Study of the CoMFA and CoMSIA models.

The QSAR study uses a predictive mathematical relationship that links the biological activity of a set of molecules to molecular descriptors (chemical properties). In the QSAR-3D approach, the PLS method is used. This method is the sequence of the multiple regression technique, with some modification of the variability of this method [38]. To establish the relationship between biological activity and the chemical descriptors of molecules, we use the methods COMFA (comparative analysis of molecular fields) and COMSIA (comparative analysis of molecular similarity indices) [39], and we calculate electrostatic and steric descriptors [40]. The COMSIA model is similar to the COMFA model, with the addition of the hydrophobic (H) descriptor and the bond donor/ acceptor Hydrogen (D/A) [41,42]. The different combinations of the 5 descriptors can build a predictive 3D-QSAR model for COMSIA with acceptable statistics.

2.3.2. Validation interne of 3D-QSAR model.

To select the best model, we use the PLS regression analysis and carry out the cross-validation leave-one-out (LOO) [43]. Selects the correct value of the cross-validation

coefficient Q^2 , the value of the correlation factor (R^2), the optimal number of NOC components, the standard error of estimate (SEE), and the F value (Fisher test). The best QSAR-3D model that selects a strong forecast should check the following conditions: $Q^2 > 0.5$, $R^2 > 0.6$, SEE lower than possible, and F greater than possible [44].

Calculation of the cross-validation factor (Q^2) and the correlation factor (R^2) by the following formula:

$$R^2 = 1 - \frac{\sum(Y_i - \hat{Y}_i)^2}{\sum(Y_i - \bar{Y}_i)^2} \quad (1)$$

$$Q^2 = 1 - \frac{\sum(Y_{pred} - Y_{exp})^2}{\sum(Y_{exp} - Y_{mean})^2} \quad (2)$$

2.3.3. External validation of 3D-QSAR models.

The QSAR-3D COMSIA model was externally validated using a test set, such as molecules that do not belong to the model development set [45]. The predictability and reliability of the generated models were assessed using a set of tests, including compounds that did not participate in the model-formation set. The external validation was carried out according to the criteria proposed by Tropsha [46,47]. It is said that the model is acceptable and predictive if it verifies the statistical criteria of Golbraikh and Tropsha [48,49].

- R_{cv}^2 Greater than 0.5;
- Greater than 0.6;
- $(R_{test}^2 - R_{0test}^2) / R_{test}^2 < 0.1$;
- $(R_{test}^2 - R_{0test}^2) / R_{test}^2 < 0.1$;
- $0.85 < k < 1.15$;
- $0.85 < k' < 1.15$;

With: R_{test}^2 : determination coefficient of test set [50]; Q^2 : The cross-validation coefficient [51]; R_0 : test: value of correlation among the values observed and those predicted; R_{0test} : The Pearson correlation coefficient among the values observed and those predicted; K: Slope of the plot of predicted versus observed activity for test set at zero intercept; k' : Slope of the plot of observed versus predicted activity at zero intercept.

2.3.4. Applicability domain.

Determining the domain of applicability (AD) is used to ensure reliable use of 3D-QSAR models [52]. The applicability domain (AD) is a virtual space within the chemical universe defined by the composition of the applied formation [23]. This technique was implemented by analyzing leverage using a Williams diagram [53], which is used to determine the activity of a structure in the test set by calculating its leverage value h and comparing it to the critical threshold h^* . The formula below is used to calculate the critical value.

$$h^* = \frac{3 \times K}{n} \quad (3)$$

$$K = p + 1. \quad (4)$$

With p : the number of descriptors in the model; n : the number of elements used to build the model [54].

2.4. Molecular docking study.

Molecular docking is a tool used in pharmaceutical research, generally performed by computer algorithms of the Auto-Dock Vina software to perform the interaction between the compound and the active site protein VIH-1 (PDB code: RT1), which was transported from the RCSB protein database [55], and then visualized the substrate-protein interactions using Discovery Studio Visualizer 2017 [56]. Positions and directions that minimize binding energy are considered the most likely and can provide information on how the substance binds to the protein [57]. This method is often used to predict the effectiveness and specificity of potential drugs before they are synthesized or experimentally tested, thereby speeding up the drug development process [58].

2.5. Molecular docking validation.

Molecular docking validation is a crucial step in ensuring the reliability of results obtained with this technique. We remove the crystal structure and redock it in the same active site of the RT1 protein, sharply compare the most stable pose with the actual co-crystallized orientation of two ligands, then calculate the average square root difference (RMSD) [59] by the following ratio, plus the low RMSD value, less than 2 Å, means a good adjustment [60].

$$RSDM(V, WT) = \sqrt{\frac{1}{2} \sum_{i=1}^n \delta^2} = \sqrt{\frac{1}{2} \sum_{i=1}^n \|V_i - w\|^2} \quad (5)$$

2.6. In silico pharmacokinetics ADMET study.

Before using a candidate drug in clinical trials, it must address ADMET's effects on absorption, distribution, metabolism, excretion, and toxicity in the human body [61, 62, 63]. The study of ADMET is costly and time-consuming [64, 65, 66]. It uses computer-assisted methods to quickly predict the ADME characteristics, including pharmacokinetic properties and toxicity, of the predicted drugs [67, 68, 69]. In this part, the ADMET study of molecules proposed as anti-HIV drugs uses SwissADMET to generate molecular formulas (cdx to SMILES) [70, 71, 72] and compose them from the SMILES-formulae treated in pkCSM, respectively [73, 74].

3. Results and Discussion

3.1. 3D-QSAR statistical results.

The discovery of new anti-HIV drugs should be targeted by 3D molecular structure descriptors that have a good influence on the active site of HIV. Using CoMFA and CoMSIA methods integrated into the SYBYL-X 2.0 software to construct 3D-QSAR models, the pEC50 results, which observe and calculate 40 molecules through CoMFA methods and various combinable CoMSIA descriptors, are shown in Table 1.

The 15 selected models are based on statistical validation criteria: model R² above 0.5 and internal Q² above 0.6, as shown in Table 2. Figure 2 shows a strong correlation between the observed and calculated anti-HIV activities. In the two models, all the points are adjacent to the diagonal to the right.

With regard to the COMFA model, it represents a good predictive model with the best statistically acceptable values: the maximum value of $Q^2 = 0.532$, a significant value of $R^2 = 0.828$, a low $SEE = 0.356$, a high value of $F = 30.115$, and a prediction value of $R^2_{pred} = 0.675$. We find in Table 1 that the eigenvalue of the prediction (Reside) is very low, with a lower percentage of 5%. We note that the steric field and influence are greater than the eclectic contribution, with respective contributions of 0.533 and 0.467, indicating that the size and shape of the compound have a large effect on the activity of these molecules.

In the CoMSIA study, for all possible combinations, the best model obtained is CoMSIA/HA, with $R^2 = 0.833$, $Q^2 = 0.721$, $SEE = 0.299$, and $NOC = 6$. The descriptors involved in this model are hydrogen (A) and hydrophobic (H) binding acceptors with relative contributions of 0.887 and 0.113, respectively. On the other hand, the model that contains the hydrogen (A) and hydrophobic (H) binding acceptor fields has acceptable statistical parameters. This means that both descriptors play a very important role in improving biological activity.

Table2. statistical parameters of CoMFA and CoMSIA.

Models	R ²	Q ²	SEE	F	NOC	R ² _{pred}	Ster	Elec	Hyd	Don	Acc
CoMFA	0.828	0.532	0.356	20.028	4	0.675	0.533	0.467	-	-	-
CoMSIA/H	0.865	0.695	0.315	26.67	5	-	-	-	1	-	-
CoMSIA/SH	0.857	0.664	0.325	24.913	5	-	0.332	-	0.668	-	-
CoMSIA/SA	0.794	0.584	0.389	16.102	3	-	0.806	-	-	-	0.194
CoMSIA/ED	0.792	0.056	0.391	15.873	3	-	-	0.797	-	0.203	-
CoMSIA/HD	0.874	0.674	0.874	28.783	6	-	-	-	0.906	0.094	-
CoMSIA/HA	0.833	0.721	0.292	31.476	6	0.618	-	-	0.887	-	0.113
CoMSIA/SEA	0.527	0.880	0.298	30.438	3	-	0.422	0.502	-	-	0.076
CoMSIA/SHD	0.870	0.621	0.309	27.934	6	-	0.327	-	0.601	0.072	-
CoMSIA/SHA	0.878	0.679	0.299	30.115	6	-	0.223	-	0.700	-	0.077
CoMSIA/SDA	0.878	0.547	0.299	30.115	5	-	0.716	-	-	0.121	0.163
CoMSIA/EHA	0.895	0.503	0.278	35.408	5	-	-	0.363	0.550	-	0.087
CoMSIA/HAD	0.885	0.666	0.291	31.989	6	-	-	-	0.864	0.035	0.101
CoMSIA/SEHA	0.931	0.562	0.226	55.893	3	-	0.170	0.341	0.402	-	0.088
CoMSIA/SHDA	0.882	0.661	0.295	31.181	6	-	0.216	-	0.669	0.021	0.094

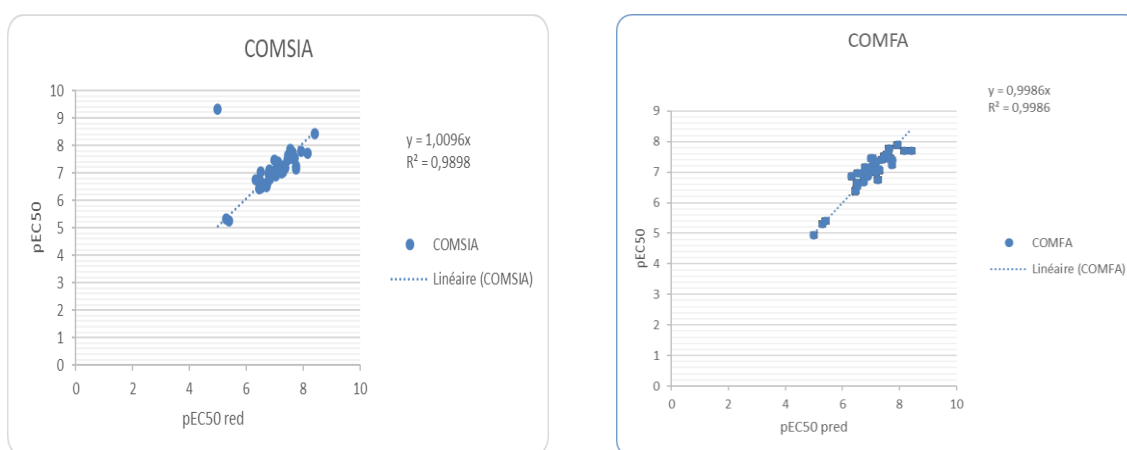


Figure 2. The correlation between pEC50 observers and pEC50 preds of the COMFA and CoMSIA models.

3.2. Validation of 3D-QSAR models.

The reliability and predictability of a model are selected based on R^2 and q^2 , as mentioned earlier, as well as external validation. For this, we have based the criteria on Globraikh and Tropsha.

Table 3 summarizes the outcomes of external validation. The correct models QSAR selects for the 8 test molecules give for the COMSFA model the values of $R^2_{pred} = 0.674$, the regression slope lines $k = 0.9921$ and $K = 1,0069$ for the inhibitor of HIV-1 activity. The values $r^2 = 0.940$ and $r'^2 = 0.982$ are used to calculate the relationships $\frac{r^2 - r_0^2}{r^2}$ and $\frac{r^2 - r_0'^2}{r^2}$. The values obtained are $-0,393$ and $-0,454$, respectively. The COMSIA model results are as follows: $R^2_{pred} = 0.62$, and the regression slope values are $k = 0.986$ and $K = 1.0124$. The values $r^2 = 0.934$ and $r_0'^2 = 0.941$ used to calculate the relationships $\frac{r^2 - r_0^2}{r^2}$ and $\frac{r^2 - r_0'^2}{r^2}$ of the values, respectively, are $-0,5107$ and $-0,5221$. After analyzing the validation results, it was found that the selected model, COMSIA/HA, is a good predictor of new molecules with improved biological activity.

Table 3. Golbraikh and Tropsha results summary.

Parameter	Formula	Threshold	3D-QSAR	
			COMFA	COMSIA
$Q^2_{training}$		$Q^2_{training} > 0.5$	0.532	0.721
r^2	Value of determination for the COMFA, COMSIA evaluates set's visualization of predicted compared to observed data.	$r^2 > 0.6$	0.674	0.62
r_0^2	r^2 the position of zero intersection		0.940	0.934
$r_0'^2$	r^2 to the experiment set's observed compared to expected activity, visualize at zero intersection		0.982	0.941
$ r_0^2 - r_0'^2 $		$ r_0^2 - r_0'^2 < 0.3$	0.042	0.070
k	Plotting the expected compared to observed activity for the test set at zero intercept and its slope	$0,85 < k < 1.15$	0.9921	0.986
$\frac{r^2 - r_0^2}{r^2}$		$\frac{r^2 - r_0^2}{r^2} < 0.1$	-0.393	-0.510
k'	Plotting the observed compared to predicted activity at the zero intersection and its slope	$0,85 < k' < 1.15$	1.006 9	1.012
$\frac{r^2 - r_0'^2}{r^2}$		$\frac{r^2 - r_0'^2}{r^2} < 0.1$	-0.454	-0.522

3.3. Domains of applicability.

The result of the scope of the QSAR3D model is illustrated in Figure 3 of the Williams plan. This result shows that the mol18 compound does not belong to the applicability area because the critical value h^* is greater than ($h^* = 0.29$), or $h^* = 3 \times K/n$, $p = 2$, $n = 32$. Except for mol18, all learning and test molecules fall within the limit interval (DA), indicating that the QSAR-3D model is well explained.

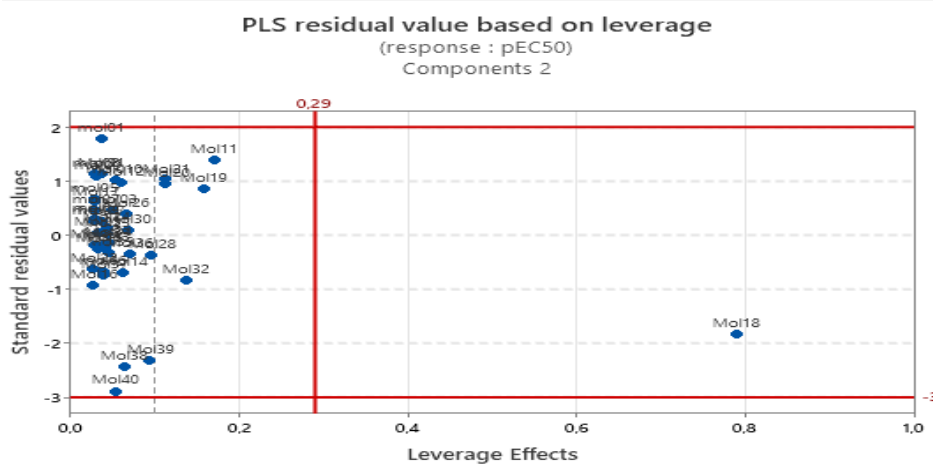


Figure 3. William's diagram of the QSAR-3D model.

3.4. Discussion of COMFA and COMSIA carts.

The COMFA and COMSIA contour visualizations enable the prediction of QSAR-3D models. The compound 11, which is the most active, is used as a reference for storyteller construction. Figure 4 and Figure 5 represent the COMSIA and COMFA contour maps.

Figure 3 shows COMFA's sterile fields. The region outlined in green is favorable for bulky groups to improve biological activity. The Juan region account shows that sterile positions decrease activity. In Figure 4, we see that the green outline near the pyridine ring indicates that adding a bulky group to R2 improves biological activity. The yellow outline near the R1 phenyl group indicates that smaller substitutes increase biological activity. The COMSIA model map shown in Figures 5a and 5b represents the hydrophobic field distribution and the COMSIA hydrogen-binding acceptor, respectively. For hydrophobic fields, Figure 5a represents yellow contours that target the regions in which the favorable hydrophobic substituent is present, and gray contours present the low-hydrophilic antiviral active regions. The yellow contour, located near the pyridine ring of the R2 substituent, highlights the importance of the alkyl group, which is hydrophobic and promotes antiviral activity in this region. In the hydrogen contour acceptor map presented in Figure 5b, the red (favorable) contours are close to the phenyl group R1 and the pyrazole group X.

The results of 3D-QSAR, in the form of a COMSIA contour map, allow for the identification of regions that improve or disadvantage the activity of compounds. A set of changes was performed on the groups R1, R2, and X, considering the characteristics of the hydrophobic and acceptor fields H, leading to the proposal of new compounds with very high antiviral activity.

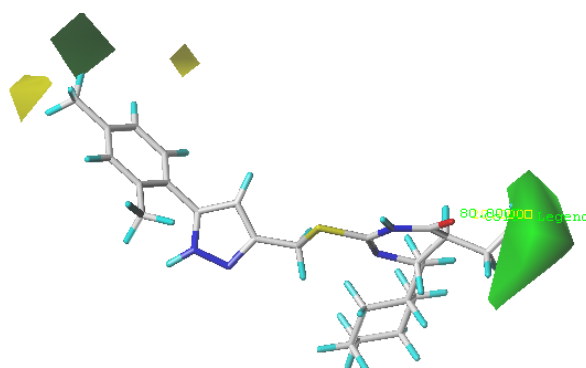


Figure 4. The green-colored ComFA map favors activity, and the yellow region disadvantages it.

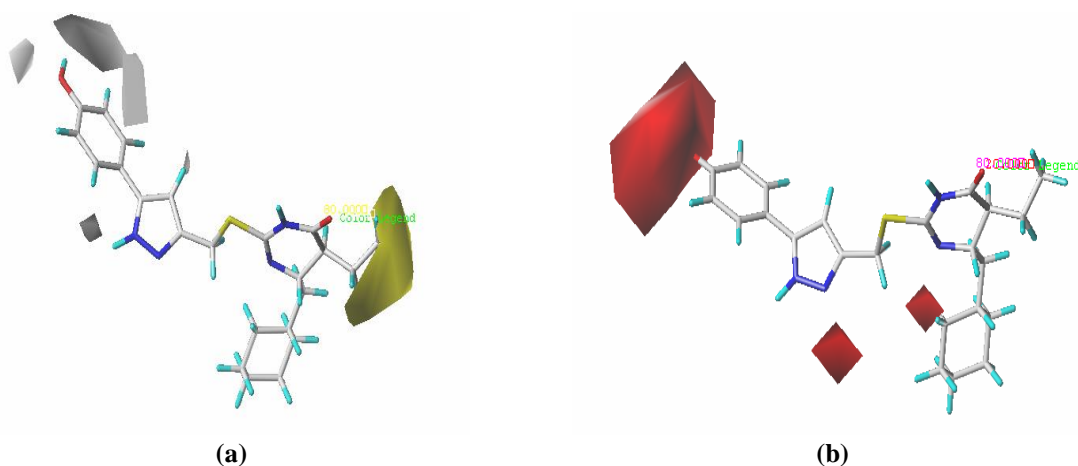


Figure 5. COMSIA contour map **5a**) hydrophobic contour; **5b**) hydrogen-accepting contour.

3.4.1. Design and results of molecular docking

To learn more about the types of molecular-protein bonds and the appropriate resistance of anti-HIV activity, we use the molecule docking procedure to determine the type of intermolecular interactions established between the 11 compounds with higher anti-HIV activity ($pEC_{50} = 7.420$) and the lowest energy levels (7.5 kcal/mol in the experimental series) and the co-crystallized protein (PDB code: 1 RT2).

The molecular docking results show that the compound 11 forms two hydrogen bonds: one between the nitrogen NH of the pyrazole ring and the amino acid ILE 270, and another between the phenolic oxygen group and the residue HIS 315, at distances of 2.19 and 1.47, respectively. There is also a hydrogen-like interaction between the oxygen phenol of compound 11 and the VAL 314 residue at a distance of 3.416. In another Pi-donor type interaction, hydrogen binds phenol and THR 351 residues of distance 2,470, and a Pi-sigma type bond between phenol and amino acid VAL 314 of distance 3,92. In addition, two interfaces of the Pi-Alkyl type are observed: the pyrazole anion entity and the PRO 272 residue, and the residue TYR 342 and the cyclohexyl group of pyrimidine have a distance of 4.56 and 4.73, respectively. The stability of this fatty compound is due to short-distance hydrogen-bonded interactions with Pi-Pi and alkyl-type bonds. Figure 6.

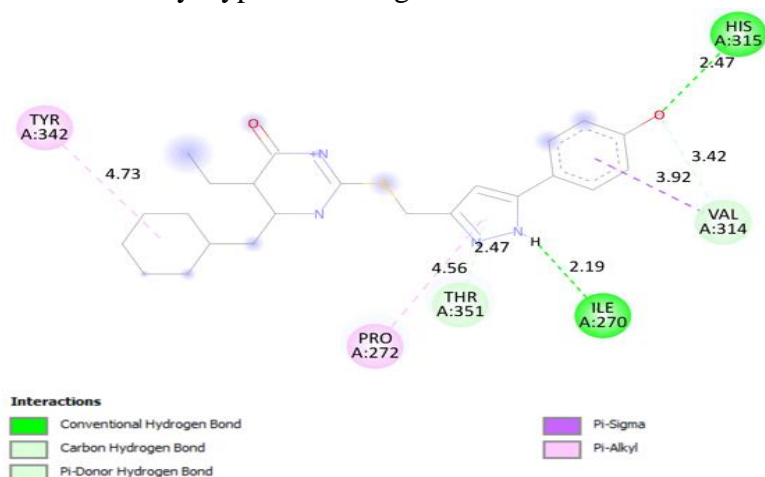


Figure 6. Molecular docking of a more active molecule of the series (compound 11).

The presence of the bonds of hydrogen types, hydrogen carbon types, and pi-donor types. Hydrogen is in the vicinity of pyrazole, which shows the hydrophile of substitutes R1 and X. The interaction of the pi-alkyl type is in the vicinity of the pyrimidine group, which explains the hydrophobicity of R2. These results are shown in the COMSIA contour map, as illustrated in Figure 7.

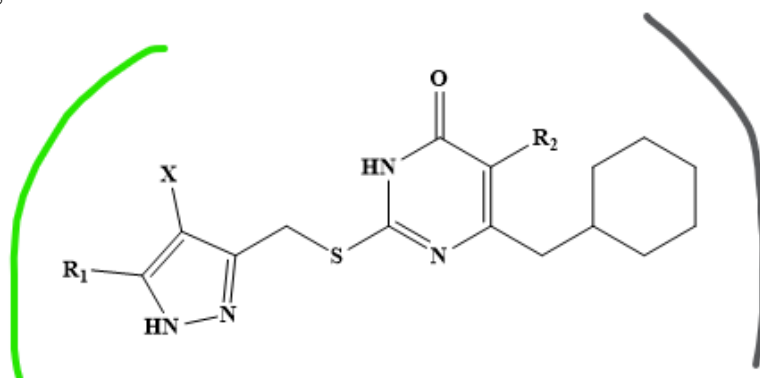


Figure 7. type of interactions by input to substitutes R1, R2, and X.

3.5. Validation of docking molecules.

We use the "re-docking" method to validate the docking procedure using the PDB's co-crystallized RT1 ligand and dock it again. It also uses Discovery Studio Visualizer 2021 to superpose the reference co-crystalline and the re-docked co-crystallized, as illustrated in Figure 8, and the calculated RMSD was 0.3166; this value of RMSD indicates the reliability of the molecular docking protocol.

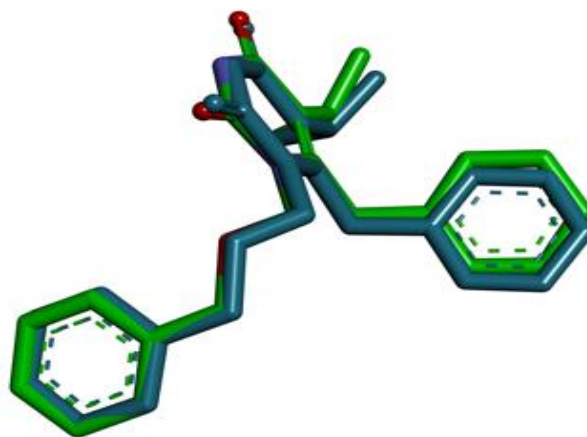


Figure 8. Type of interactions by input to substitutes R1, R2, and X.

3.6. Prediction of the new antiviral component.

The prediction of new potent anti-HIV-1 molecules is based on the 3D-QSAR model, which provides information on modifications introduced to substitutes (R1, R2, and X) of the more active base molecule 11 to raise the anti-HIV activity of parasol-pyridine. The six proposed substances are listed in Table 4, which shows their structural data and HIV biological activity, which is higher than that of our base molecule. We find that the activity pEC₅₀ of the substance Pred 21 is 11,566, indicating it is a potent antiviral.

The results in Table 4 show that the predicted activity was higher than the experimental activity, indicating that the selected models are well explanatory. Comparing the predictive values of pEC₅₀, the experimental results show the effect of hydrophobic descriptors and H hydrogen acceptors. To understand the nature of interactions between the proposed compounds and the active site of the HIV-1 protein and to assess candidate affinity, molecular docking is proposed.

The results of molecular docking for the compounds Pred21, Pred22, Pred3, Pred10, Pred1, and Pred16 were aligned with the active site of the HIV-1 (RT 1) protein. To understand the type of interaction between the substrate and the protein and select the amino acids to interact in biological activity, these results show that all predicted compounds have high affinity values between -7.7 and -9.2 kcal/mol, which is higher than the base molecule 11 at a rate of -7.7 kcal/ mol Table 4.

For the most active recommended compound Pred21 of pEC₅₀=11,566 and high affinity -8,6 kcal/mol, the grouping of NO₂ introduced at R2 and X positions plays an important role in establishing the binding of hydrogen with the amino acid GLN 269 at a distance of (2,33 Å) and (2,32 Å), respectively, and another hydrogen binding with the oxygen group pyridine and amino acids LYS350 (5,51Å), other Pi-Sigma, Pi-Alkyl and Alkyl types of binding between the amin acids TRP266, ALA355 and ILE270, and cyclohexane isopropyl at the substitution position R2, plus Pi-sulfur type interactions between the sulfur sulfur group and

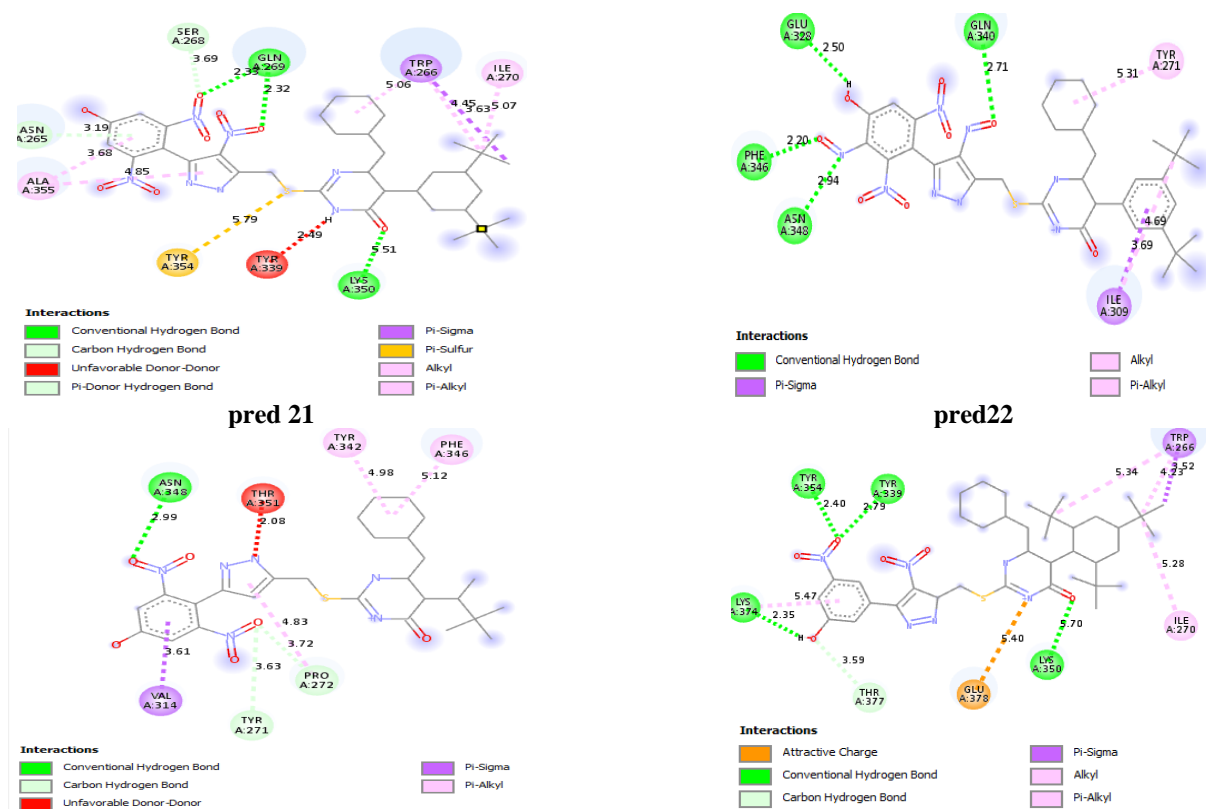
amine acid TYR4354 (TYR45.77) and an interactive type of pyridoxine at the donor group of R2 (239) Figure 9.

The substance Pred 22 of pEC50=11,543 and affinity -8,6 kcal/mol represents four hydrogen class bonds between the amino acids GLN340 (2.72 Å) with NO at replacement X positions, PHE346 (2.20 Å), ASN348 (2.94 Å), with NO and GLU328 (2.50 Å) and OH at R1 position, and other Pi-Sigma Alkyl and Pi-Alkyl type interactions between the amines ILE 309 (3.69Å), ILE309 (3,68Å) and TYR271 (5.30Å) respectively and the radical R2. (Figure 9).

For the pred2 compound of pEC50 = 11,09 and of an affinity of -7,8 kcal/mol, establish a category of hydrogen binding between the ASN348 and NO₂ residues at a distance of 2.99 Å. The phenyl oxygen meth has two hydrogen-carbon bonds between the amino acids TYR271 (3.63 Å) and PRO272 (3.72 Å) and NO₂ in the phenolic ortho, these interactions at the R1 radical position, three other Pi-Alkyl type interactions between the PRO 272 amino acid (4.83 Å) and the pyrazole nucleus, and two more between the cyclohexane group and the PHE346 group (5.12 Å), TYR342 (5 Å) in the R2 replacement region, plus a donor-donor unfavorable interaction between Pyrazole nitrogen and the amino acid THR351 (2.08 Å) (Figure 9).

Other molecular redocking results of the compounds Pred10, Pred1 and Pred16 represented hydrogen-type interactions between TYR354(2.40Å), TYR339(2,79Å), LYS374 (2.35Å), LYS350 (5,70Å) and TRP535 (2,02 Å) (2,57), LEU533 (2,53 Å), ILE506 (2,35 Å), GLN507 (2,78Å), and TYR232(2,18 Å) (2,72 Å), HIS96 (2,18Å) respectively at the X and R1 substitutes, and Pi-Sigma, Alkyl and pi-Alkyl type interactions with residues TRP266, ILE270, LEI525, ILE550, LEU425, ALA534, TRP266, ILE382 Figure 9.

These results validate the data obtained from the contour map of the COMSIA model. Specifically, hydrogen bond acceptors at the X and R1 positions explain the addition of groups such as NO₂, NH₃, and OH. Additionally, hydrophobic fields at the R2 positions favor the inclusion of bulky groups, indicating that these compounds exhibit stronger hydrogen bonding, as shown in Figure 9.



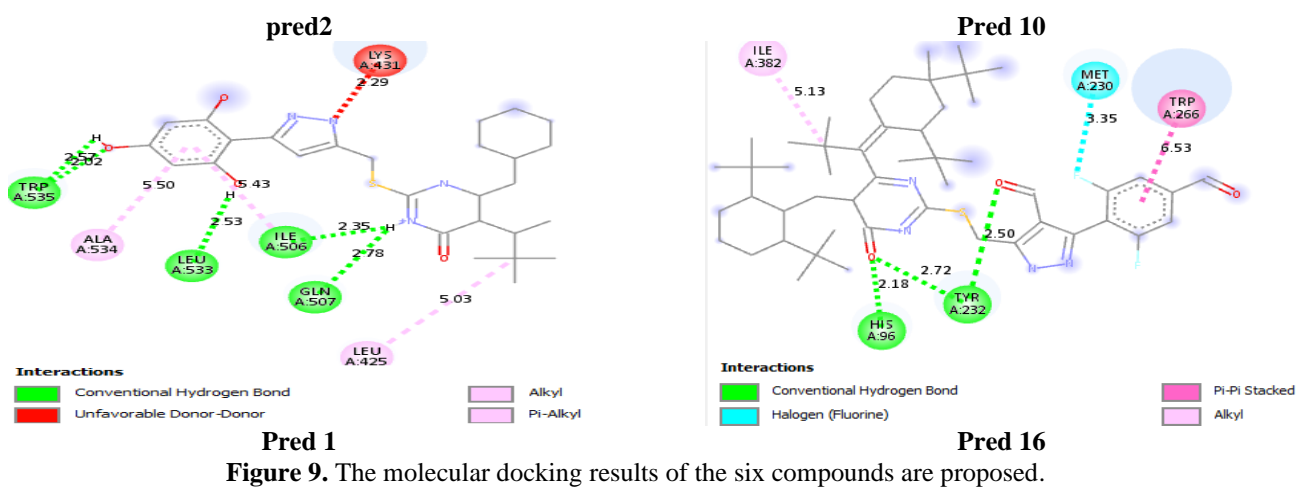
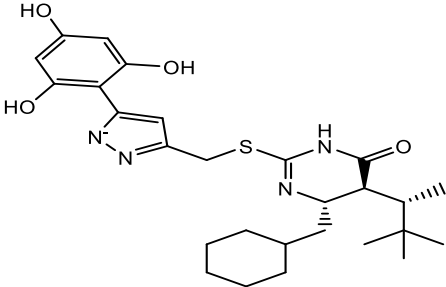
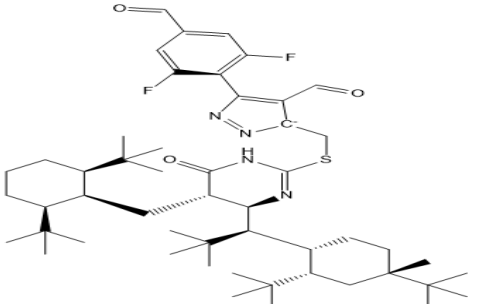


Figure 9. The molecular docking results of the six compounds are proposed.

Table 4. The six new compounds proposed by CoMSIA/SH have predicted antiviral activities.

Compounds	Structure	pEC50 pred CoMSIA/HA	Affinity
Pred 21		11.566	-8.6
Pred 22		11.543	-8.6
Pred2		11,09	-9.2
Pred 10		9,762	-7.8

Compounds	Structure	pEC50 pred CoMSIA/HA	Affinity
Pred 1		9.334	-7.9
Pred 16		9.026	-7.7

3.7. Free binding energy MMGBSA results,

The binding free energy of the protein with the designed compounds was estimated using the MMGBSA method, specifically the MM-GBSA Prime module in Schrödinger (2021) [75]. The average binding energies are presented in Table 5. For the complexes with Pred 21, Pred 22, Pred2, Pred 10, Pred 1, and Pred 16, the average binding free energies were found to be -76.6880, -76.7220, -69.9178, -61.5673, -61.5556, and -59.4106, respectively. Among these, Pred 21 and Pred 22 showed particularly notable binding free energies.

Table 5. Results of molecular docking and MMGBSA of newly designed compounds.

Comp. No.	ΔG_{vdW}	$\Delta G_{Solv GB}$	$\Delta G_{Packing}$	ΔG_{Lipo}	ΔG_{Hbond}	$\Delta G_{Covalent}$	$\Delta G_{Coulomb}$	ΔG_{bind}
Pred 21	-37.2621	22.0181	-7.3022	-16.3277	-6.8843	1.7639	-26.1123	-86.6880
Pred 22	-33.9815	25.4977	-1.2019	-13.9397	-3.0894	3.3279	-26.8902	-826.7220
Pred2	-27.2092	25.5325	-9.9706	-16.2174	-4.8532	7.1667	-22.5525	-69.9178
Pred 10	-27.4011	33.5748	-3.0869	-16.5490	-3.0920	10.0399	-25.02783	-61.5673
Pred 1	-26.9019	24.3219	-5.6134	-15.8077	-3.99247	8.7684	-23.0100	-61.5556
Pred 16	-26.1456	26.1443	-9.4707	-15.2028	-4.1024	9.8112	-21.0161	-59.4106

Additionally, the analysis of energetic components revealed that van der Waals interactions (ΔG_{vdW}), the packing fraction ($\Delta G_{Packing}$), lipophilic interactions (ΔG_{Lipo}), and Coulomb interactions ($\Delta G_{Coulomb}$) all favored the formation of the protein-ligand complex. In contrast, binding solvation GB and covalent binding ($\Delta G_{Covalent}$) showed more positive values, opposing complex formation. The free energy data further indicate that van der Waals interactions play a significant role in stabilizing the protein-ligand complexes across all the studied systems.

3.8. ADMET results.

The bioavailability verification of compounds proposes Pred22, Pred02, Pred10, Pred22, Pred1, and Pred16 to perform a predictive study of pharmacokinetic properties (ADMET) based on the results of the calculation of the pharmacokinetic parameters absorption, distribution, metabolism, excretion, and toxicity represented in Table 6.

The solubility values are acceptable as they range between -4.39 and -2.932 log (mol/L) [75]. The proposed substance has acceptable water solubility; the five substances have better absorption, greater than 81.24%, which shows that these compounds have excellent absorption [76], and the five predicted substances have values of drug volume distribution in the tissues of the organism (VDss) that are not small, because if these values are above 0.45, it is said that the distribution volume is important; if less than -0.15 is small [77], all the proposed compounds have values less than -0.15, thus their volume of distribution is small. For the prediction of the pharmacokinetics and transformation of these substances in the membranes of the body, the values of blood-brain barrier permeability (BBB) are greater than -2.335; in addition, the Central Nervous System (CNS) permeability values for all compounds have values (Log PS) greater strictly than -3, which means that these compounds are able to penetrate the CNS[70].

Metabolism is the set of chemical reactions that occur between the drug and the human body; the enzyme cytochrome CYP450 is responsible for detoxification and oxidizes the metabolite for extraction [78]. There are several types of CYP-type enzymes, including CYPs1, CYP2, CYP3, and CYP4, with a proportion of more than 90%, and the enzyme responsible for the biotransformation of drugs 1A2, 2C9, 2C19, 2D6, and 3A4 [75]. In this study, the metabolism results are acceptable for all predicted compounds, which are CYP3A4 substrates except the compound pred1, but no compound of the substrate type CYB2D6; those relating to the inhibitor CYP3A4; all inhibitors of the CYP3A4-Type except for the substances Pred2 and Pred10 are CYP2C9 inhibitors. The clarity of the five compounds is low but acceptable, indicating that the drug persists in the body [79]. The results of AMES toxicity and AMES skin toxicity are used to check the toxicities of the drugs; all the proposed compounds are non-toxic.

Table 6. The expected outcome of ADMET compounds is predicted.

N°	Absorption		Distribution			Metabolism							Excretion	Toxicity
	Intestinal	Water solubility (human)	VDSS (human)	BBB permeability	CNS permeability	substrate		inibiteur						
	absorption					CYP								
	(human)	Numeric (% Absorbed)	Numeric (Log L/kg)	Numeric (Log BB)	Numeric (Log PS)	2D6	3A4	1A2	C19	2C9	2D6	3A4	(Log ml/min/kg)	Categorical (Yes/No)
Pred 22	97.673	-4.39	-0.895	-2.335	-1.629	No	Yes	No	No	No	No	Yes	-0.045	No
Pred 21	95.781	-4.42	-0.715	-2.126	-1.659	No	Yes	No	No	No	No	Yes	0.036	yes
Pred 2	92.728	-4.147	-0.725	-1.04	-2.229	No	Yes	No	Yes	Yes	No	Yes	0.422	No
Pred 10	85.424	-3.084	-1.557	-1.691	-2.808	No	Yes	No	No	yes	No	No	-0,055	No
Pred 1	81.249	-3,84	-0.025	-1.494	-2.391	No	Yes	No	Yes	Yes	No	No	0.172	No
Pred 16	97.666	-2.932	-1.25	-0.242	-1.984	No	Yes	No	No	No	No	Yes	-0.784	No

According to the ADMET results, prodrug compounds exhibit better adsorption, distribution, permeability, metabolism, and non-toxicity, and have low clearance values, suggesting that these proposed compounds are candidates for anti-HIV.

4. Conclusions

This work presents a study of 3D-QSAR modeling using the COMFA and COMCIA methods to construct a predictive QSAR model that links the chemical properties of a pyrazolyl-pyrimidinone series with biological antiviral activity, thereby predicting new potent molecules against HIV-1. Model validation is carried out by internal, external, and domain application methods to verify the reliability of the proposed models, CoMSIA/HA, and CoMFA/E+S. We find good statistical values for CoMFA ($Q^2 = 0.828$, $R^2 = 0.532$, $R^2_{pred} = 0.675$) and CoMSIA/HA ($Q^2 = 0.833$, $R^2 = 0.721$, $R^2_{pre} = 0.681$). According to the contour maps, the selected model, CoMSIA/HA, meets the external validation criteria of Golbraikh-Tropsha. This model proposes six compounds with good antiviral activity, stronger than that of the base N11. On the other hand, a molecular docking study performed on the proposed six compound showed good stability of the ligand-protein interaction complexes and a low value of RMSD. Also, the six composite showed good predictive performance for ADMET pharmacokinetics and toxicity. Based on these results, it was concluded that these proposed compounds represent the best new HIV drug candidate.

Author Contributions

Conceptualization, B.H. and K.T.; methodology, B.H. and S.Z.; software, M.D.; validation, K.M., K.O., and M.E.; formal analysis, K.T.; investigation, S.Z. and M.E.; writing—original draft preparation, K.T.; writing—review and editing, B.H. and K.M.; visualization, K.O.; supervision, B.H., M.E., and H.O.; project administration, B.H. All authors have read and agreed to the published version of the manuscript.

Institutional Review Board Statement

Not applicable.

Informed Consent Statement

Not applicable.

Data Availability Statement

Data supporting the findings of this study are available upon reasonable request from the corresponding author.

Funding

This research received no external funding.

Acknowledgments

We are grateful to the “Association Marocaine des Chimistes Théoriciens” (AMCT) for its valuable assistance regarding the programs.

Conflicts of Interest

The authors declare that they have no known competing financial interests or personal relationships that could have influenced the work reported in this paper.

References

1. Hazenberg, M.D.; Hamann, D.; Schuitemaker, H.; Miedema, F. T cell depletion in HIV-1 infection: how CD4⁺T cells go out of stock. *Nature Immunology* **2000**, *1*, 285-289, <https://doi.org/10.1038/79724>.
2. Zhan, P.; Liu, X.; Li, Z.; Pannecouque, C.; De Clercq, E. Design Strategies of Novel NNRTIs to Overcome Drug Resistance. *Current Medicinal Chemistry* **2009**, *16*, 3903–3917, <https://doi.org/10.2174/092986709789178019>.
3. Adamson, C.S.; Freed, E.O. Novel Approaches to Inhibiting HIV-1 Replication. *Antiviral research* **2010**, *85*, 119-141, <https://doi.org/10.1016/j.antiviral.2009.09.009>.
4. Sever, B.; Otsuka, M.; Fujita, M.; Ciftci, H. A Review of FDA-Approved Anti-HIV-1 Drugs, Anti-Gag Compounds, and Potential Strategies for HIV-1 Eradication. *Int. J. Mol. Sci.* **2024**, *25*, 3659, <https://doi.org/10.3390/ijms25073659>.
5. Desai, K.; Arora, P. Chapter 5 - Burden of infectious diseases and strategies of prevention. In *Viral, Parasitic, Bacterial, and Fungal Infections*, Bagchi, D., Das, A., Downs, B.W., Eds.; Academic Press: **2023**; pp. 49-61, <https://doi.org/10.1016/B978-0-323-85730-7.00052-7>.
6. Ding, X.; Cui, R.; Yu, J.; Liu, T.; Zhu, T.; Wang, D.; Chang, J.; Fan, Z.; Liu, X.; Chen, K. Active learning for drug design: a case study on the plasma exposure of orally administered drugs. *Journal of Medicinal Chemistry* **2021**, *64*, 16838-16853, <https://doi.org/10.1021/acs.jmedchem.1c01683>.
7. Sarafianos, S.G.; Marchand, B.; Das, K.; Himmel, D.M.; Parniak, M.A.; Hughes, S.H.; Arnold, E. Structure and function of HIV-1 reverse transcriptase: molecular mechanisms of polymerization and inhibition. *Journal of Molecular Biology* **2009**, *385*, 693-713, <https://doi.org/10.1016/j.jmb.2008.10.071>.
8. Talbi, S.; Dib, M.; Bouissane, L.; Abderrafia, H.; Rabi, S.; Khouili, M. Recent Progress in the Synthesis of Heterocycles based on 1, 3-diketones. *Current Organic Synthesis*, **2022**, *19*(2), 220-245.
9. Farouki, K. E.; Kacem, M.; Dib, M.; Ouchetto, H.; Hafid, A.; Khouili, M. A review on the recent progress of layered double hydroxides (LDHs)-based catalysts for heterocyclic synthesis. *Current Organocatalysis*, **2024**, *11*(2), 154-174. <https://doi.org/10.2174/0122133372264682231019101634>.
10. Akhramez, S.; Achour, Y.; Dib, M.; Bahsis, L.; Ouchetto, H.; Hafid, A.; Khouili, M.; El Haddad, M. DFT study and synthesis of novel bioactive bispyrazole using Mg/Al-LDH as a solid base catalyst. *Curr. Chem. Biol.*, **2021**, *14*(4), 240-249. <http://dx.doi.org/10.2174/2212796814999200918175018>.
11. Hatim, C.; Boussetta, A.; Kacem, M.; Mustapha Dib, M.; Ouchetto, K.; Hafid, A.; Khouili, M.; Ouchetto, H. Thiazolidine Derivatives: An Up-to-Date Review of Synthesis and Biological Activity. *Curr. Top. Med. Chem.*, **2025**. <http://dx.doi.org/10.2174/0115680266386939250917053818>.
12. Mitchell, S.C.; Steventon, G.B. Thiourea and Its Biological Interactions. *Sulfur reports Taylor & Francis*: **1994**, *16*, 117–137, <https://doi.org/10.1080/01961779408048967>.
13. Ahmad, G.; Sohail, M.; Bilal, M.; Rasool, N.; Qamar, M.U.; Ciurea, C.; Marceanu, L.G.; Misarca, C. N-Heterocycles as promising antiviral agents: a comprehensive overview. *Molecules* **2024**, *29*, 2232, <https://doi.org/10.3390/molecules29102232>.
14. Barreiro, G.; Guimarães, C.R.W.; Tubert-Brohman, I.; Lyons, T.M.; Tirado-Rives, J.; Jorgensen, W.L. Search for Non-nucleoside Inhibitors of HIV-1 Reverse Transcriptase using Chemical Similarity, Molecular Docking, and MM-GB/SA Scoring. *Journal of Chemical Information and Modeling* **2007**, *47*, 2416–2428, <https://doi.org/10.1021/ci700271z>.
15. Hritzová, O.; Kutschy, P.; Imrich, J.; Schöffmann, T. Hydrogen bonds in N-(3-chloro-2-benzo[b]thienocarbonyl)- and N-(2-benzo[b]thienocarbonyl)-N'-monosubstituted thioureas. *Collect. Czech. Chem. Commun.* **1987**, *52*, 2673–2679, <https://doi.org/10.1135/cccc19872673>.
16. Zhou, Z.; Lin, X.; Madura, J.D. HIV-1 RT Non-nucleoside Inhibitors and Their Interaction with RT for Antiviral Drug Development. *Infectious Disorders - Drug TargetsDisorders* **2006**, *6*, 391–413, <https://doi.org/10.2174/187152606779025833>.
17. Artico, M.; Massa, S.; Mai, A.; Marongiu, M.; Piras, G.; Tramontano, E.; La Colla, P. 3, 4-Dihydro-2-alkoxy-6-benzyl-4-oxypyrimidines (DABOs): a new class of specific inhibitors of human

- immunodeficiency virus type 1. *Antiviral Chemistry and Chemotherapy* **1993**, *4*, 361-368, <https://doi.org/10.1177/095632029300400608>.
18. D'cruz, O.J.; Uckun, F.M. Novel tight binding PEST, HEPT and DABO-based non-nucleoside inhibitors of HIV-1 reverse transcriptase. *Journal of enzyme inhibition and medicinal chemistry* **2006**, *21*, 329-350, <https://doi.org/10.1080/14756360600774413>.
 19. Mai, A.; Artico, M.; Sbardella, G.; Massa, S.; Novellino, E.; Greco, G.; Loi, A.G.; Tramontano, E.; Marongiu, M.E.; La Colla, P. 5-Alkyl-2-(alkylthio)-6-(2,6-dihalophenylmethyl)-3,4-dihydropyrimidin-4(3H)-ones: Novel Potent and Selective Dihydro-alkoxy-benzyl-oxopyrimidine Derivatives. *Journal of Medicinal Chemistry* **1999**, *42*, 619-627, <https://doi.org/10.1021/jm980260f>.
 20. He, Y.; Chen, F.; Sun, G.; Wang, Y.; De Clercq, E.; Balzarini, J.; Pannecouque, C. 5-Alkyl-2-[(aryl and alkyloxylcarbonylmethyl) thio]-6-(1-naphthylmethyl) pyrimidin-4 (3H)-ones as an unique HIV reverse transcriptase inhibitors of S-DABO series. *Bioorganic & medicinal chemistry letters* **2004**, *14*, 3173-3176, <https://doi.org/10.1016/j.bmcl.2004.04.008>.
 21. He, Y.; Chen, F.; Yu, X.; Wang, Y.; De Clercq, E.; Balzarini, J.; Pannecouque, C. Non-nucleoside HIV-1 reverse transcriptase inhibitors; part 3. Synthesis and antiviral activity of 5-alkyl-2-[(aryl and alkyloxyl-carbonylmethyl) thio]-6-(1-naphthylmethyl) pyrimidin-4 (3H)-ones. *Bioorganic chemistry* **2004**, *32*, 536-548, <https://doi.org/10.1016/j.bioorg.2004.05.007>.
 22. Long, J.; Zhang, D.; Zhang, G.; Rao, Z.; Wang, Y.; Tam, S.; He, Y.; Zheng, Y. The anti-HIV activity of three 2-alkylsulfanyl-6-benzyl-3, 4-dihydropyrimidin-4 (3H)-one derivatives acting as non-nucleoside reverse transcriptase inhibitor in vitro. *Yao xue xue bao* **2010**, *45*, 228-234.
 23. Rao, Z.-K.; Long, J.; Li, C.; Zhang, S.-S.; He, M.; Ou, L.-C.; Zheng, Y.-T.; He, Y.-P. Synthesis and anti-HIV-1 activity of S-dihydro (alkyloxy) benzyloxy pyrimidine derivatives. *Monatshefte für Chemie-Chemical Monthly* **2008**, *139*, 967-974, <https://doi.org/10.1007/s00706-007-0834-8>.
 24. Hamdache, B., Tabti, K., Er-rajy, M., Dib, M., ElFarouki, K., Ouchetto, K., ... & Ouchetto, H. QSAR Modeling and Molecular Docking Studies of New Substituted Pyrazolyl-Pyrimidinones as Potent HIV-1 Inhibitors. *Current Chemical Biology*, **2024**, *18*(3), 157-175. <https://doi.org/10.2174/0122127968317638241014090751>.
 25. Kciuk, M.; Gielecińska, A.; Mujwar, S.; Mojzych, M.; Marciniak, B.; Drozda, R.; et al. Targeting carbonic anhydrase IX and XII isoforms with small molecule inhibitors and monoclonal antibodies. *Journal of Enzyme Inhibition and Medicinal Chemistry*, **2022**, *37*(1), 1278-1298 <https://doi.org/10.1080/14756366.2022.2052868>.
 26. Radosveta G. Elias S.J. A. Thioredoxin Reductase Inhibition for Cancer Therapy. *Annual Reviews*. **2022**, *62*, 177-196, <https://doi.org/10.1146/annurev-pharmtox-052220-102509>.
 27. Abdessadak, O.; Tabti, K.; Alaqrbeh, M.; Elmchichi, L.; Koubi, Y.; Sbai, S.; Ajana, M.A.; Lakhlifi, T.; Bouachrine, M. Computational Studies for Development of Triazole-Pyrimidines as Inhibitor of α -Tubulin Receptor. *ChemistrySelect* **2023**, *8*, e202301992, <https://doi.org/10.1002/slct.202301992>.
 28. Tabti, K.; Elmchichi, L.; Sbai, A.; Maghat, H.; Bouachrine, M.; Lakhlifi, T.; Ghosh, A. In silico design of novel PIN1 inhibitors by combined of 3D-QSAR, molecular docking, molecular dynamic simulation and ADMET studies. *Journal of Molecular Structure* **2022**, *1253*, 132291, <https://doi.org/10.1016/j.molstruc.2021.132291>.
 29. Vora, J.; Patel, S.; Sinha, S.; Sharma, S.; Srivastava, A.; Chhabria, M.; Shrivastava, N. Structure based virtual screening, 3D-QSAR, molecular dynamics and ADMET studies for selection of natural inhibitors against structural and non-structural targets of Chikungunya. *Journal of Biomolecular Structure and Dynamics* **2019**, *37*, 3150-3161, <https://doi.org/10.1080/07391102.2018.1509732>.
 30. Tabti K, Baammi S, ElMchichi L, Sbai A, Maghat H, Bouachrine M, Lakhlifi T Computational investigation of pyrrolidin derivatives as novel GPX4/MDM2-P53 inhibitors using 2D/3DQSAR, ADME/Toxicity, molecular docking, molecular dynamics simulations, and MM-GBSA free energy. *Struct Chem* **2022**, *33*, 1019-1039, <https://doi.org/10.1007/s11224-022-01903-5>.
 31. Xu, X.; Wang, J.; Yao, Q. Synthesis and quantitative structure-activity relationship (QSAR) analysis of some novel oxadiazolo[3,4-d]pyrimidine nucleosides derivatives as antiviral agents. *Bioorganic & Medicinal Chemistry Letters* **2015**, *25*, 241-244, <https://doi.org/10.1016/j.bmcl.2014.11.065>.
 32. Abdullahi, S.H.; Moin, A.T.; Uzairu, A.; Umar, A.B.; Ibrahim, M.T.; Usman, M.T.; Nawal, N.; Bayil, I.; Zubair, T. Molecular docking studies of some benzoxazole and benzothiazole derivatives as VEGFR-2 target inhibitors: In silico design, MD simulation, pharmacokinetics and DFT studies. *Intelligent Pharmacy* **2024**, *2*, 232-250, <https://doi.org/10.1016/j.ipha.2023.11.010>.

33. Mitra, I.; Saha, A.; Roy, K. Development of multiple QSAR models for consensus predictions and unified mechanistic interpretations of the free-radical scavenging activities of chromone derivatives. *Journal of Molecular Modeling* **2012**, *18*, 1819–1840, <https://doi.org/10.1007/s00894-011-1198-x>.
34. Varpe, B.D.; Jadhav, S.B.; Chatale, B.C.; Mali, A.S.; Jadhav, S.Y.; Kulkarni, A.A. 3D-QSAR and Pharmacophore modeling of 3,5-disubstituted indole derivatives as Pim kinase inhibitors. *Structural Chemistry* **2020**, *31*, 1675–1690, <https://doi.org/10.1007/s11224-020-01503-1>.
35. El fadili, M.; Er-rajy, M.; Imtara, H.; Kara, M.; Zarougui, S.; Altwaijry, N.; Al kamaly, O.; Al Sfouk, A.; Elhallaoui, M. 3D-QSAR, ADME-Tox in silico prediction and molecular docking studies for modeling the analgesic activity against neuropathic pain of novel NR2B-selective NMDA receptor antagonists. *Processes* **2022**, *10*, 1462, <https://doi.org/10.3390/pr10081462>.
36. Roy, K.; Kar, S.; Ambure, P. On a simple approach for determining applicability domain of QSAR models. *Chemometrics and Intelligent Laboratory Systems* **2015**, *145*, 22–29, <https://doi.org/10.1016/j.chemolab.2015.04.013>.
37. Urig, S.; Becker, K. On the potential of thioredoxin reductase inhibitors for cancer therapy. *Seminars in Cancer Biology* **2006**, *16*, 452–465, <https://doi.org/10.1016/j.semcancer.2006.09.004>.
38. Tabti, K.; Elmchichi, L.; Sbai, A.; Maghat, H.; Bouachrine, M.; Lakhlifi, T. HQSAR, CoMFA, CoMSIA docking studies and simulation MD on quinazolines/quinolines derivatives for DENV virus inhibitory activity. *Chem Afr.* **2022**, *5*, 1937–1958, <https://doi.org/10.1007/s42250-022-00484-4>.
39. Mujwar, S.; Pardasani, K.R. Prediction of riboswitch as a potential drug target and design of its optimal inhibitors for Mycobacterium tuberculosis. *International Journal of Computational Biology and Drug Design* **2015**, *8*, 326–347, <https://doi.org/10.1504/IJCBDD.2015.073671>.
40. Jain, R.; Mujwar, S. Repurposing metocurine as main protease inhibitor to develop novel antiviral therapy for COVID-19. *Structural Chemistry* **2020**, *31*, 2487–2499, <https://doi.org/10.1007/s11224-020-01605-w>.
41. Shinu, P.; Sharma, M.; Gupta, G.L.; Mujwar, S.; Kandeel, M.; Kumar, M.; Nair, A.B.; Goyal, M.; Singh, P.; Attimarad, M. Computational design, synthesis, and pharmacological evaluation of naproxen-guaiacol chimera for gastro-sparing anti-inflammatory response by selective COX2 inhibition. *Molecules* **2022**, *27*, 6905, <https://doi.org/10.3390/molecules27206905>.
42. Hajji, H.; Tabti, K.; En-nahli, F.; Bouamrane, S.; Lakhlifi, T.; Ajana, M.A.; Bouachrine, M. In silico investigation on the beneficial effects of medicinal plants on diabetes and obesity: molecular docking, molecular dynamic simulations, and ADMET studies. *Biointerface Res Appl Chem* **2021**, *11*, 6933–6949, <https://doi.org/10.33263/BRIAC115.69336949>.
43. Mendes, G.O.; Araújo Neto, M.F.; Barbosa, D.B.; Bomfim, M.R.; Andrade, L.S.; Carvalho, P.B.; Oliveira, T.A.; Falkoski, D.L.; Maia, E.H.; Valle, M.S.; Damázio, L.C.; Silva, A.M.; Taranto, A.G.; Leite, F.H. Identification of Potential Multitarget Compounds against Alzheimer's Disease through Pharmacophore-Based Virtual Screening. *Pharmaceuticals* **2023**, *16*, 1645, <https://doi.org/10.3390/ph16121645>.
44. Elbouhi, M.; Tabti, K.; Ouabane, M.; Alaqarbeh, M.; Elkamel, K.; Lakhlifi, T.; Sbai, A.; Bouachrine, M. A computational exploration of the antioxidant potential of conjugated quinazolinone Schiff bases. *Chemistry of Heterocyclic Compounds* **2024**, *60*, 627–638, <https://doi.org/10.1007/s10593-025-03386-8>.
45. Tabti, K.; Mchichi, L.E.; Sbai, A.; Maghat, H.; Bouachrine, M.; Lakhlifi, T. 2D and 3D-QSAR/CoMSIA Comparative Study On a Series of Thiazole Derivatives as SDHI Inhibitors. *Maghrebian Journal of Pure and Applied Science* **2020**, *6*, 73–90, <https://doi.org/10.48383/IMIST.PRSM/mjpas-v6i2.23108>.
46. Parkali, P.M.; Shyam Kumar, A.; Johanna K, P.; Prodensia T, S.; Turaga, S.; Shaiva, V.; Pujar, G.V.; Joshi, S.D.; Aminabhavi, T.M.; Dixit, S.R. Molecular docking and three-dimensional quantitative structure–activity relationships for antitubercular pyrimidine derivatives. *Polycyclic Aromatic Compounds* **2022**, *42*, 4132–4145, <https://doi.org/10.1080/10406638.2021.1885455>.
47. Klebe, G.; Abraham, U.; Mietzner, T. Molecular similarity indices in a comparative analysis (CoMSIA) of drug molecules to correlate and predict their biological activity. *Journal of Medicinal Chemistry* **1994**, *37*, 4130–4146, <https://doi.org/10.1021/jm00050a010>.
48. Sepehri, A.; Sarrafzadeh, M.-H. Effect of nitrifiers community on fouling mitigation and nitrification efficiency in a membrane bioreactor. *Chemical Engineering and Processing - Process Intensification* **2018**, *128*, 10–18, <https://doi.org/10.1016/j.cep.2018.04.006>.
49. Abdizadeh, R.; Hadizadeh, F.; Abdizadeh, T. QSAR analysis of coumarin-based benzamides as histone deacetylase inhibitors using CoMFA, CoMSIA and HQSAR methods. *Journal of Molecular Structure* **2020**, *1199*, 126961, <https://doi.org/10.1016/j.molstruc.2019.126961>.

50. Abdizadeh, T.; Ghodsi, R.; Hadizadeh, F. 3D-QSAR (CoMFA, CoMSIA) and Molecular Docking Studies on Histone Deacetylase 1 Selective Inhibitors. *Recent Patents on Anti-Cancer Drug Discovery* **2017**, *12*, 365–383, <https://doi.org/10.2174/1574892812666170508125927>.
51. El Masaoudy, Y.; Tabti, K.; Koubi, Y.; Maghat, H.; Lakhlifi, T.; Bouachrine, M. In silico design of new pyrimidine-2, 4-dione derivatives as promising inhibitors for HIV Reverse Transcriptase-associated RNase H using 2D-QSAR modeling and (ADME/Tox) properties. *Moroc. J. Chem.* **2023**, *11*, 300–317, <https://doi.org/10.48317/IMIST.PRSM/morjchem-v11i2.35455>.
52. Chicco, D.; Warrens, M.J.; Jurman, G. The coefficient of determination R-squared is more informative than SMAPE, MAE, MAPE, MSE and RMSE in regression analysis evaluation. *Peerj computer science* **2021**, *7*, e623, <https://doi.org/10.7717/peerj-cs.623>.
53. Kumar, P.; Kumar, A.; Sindhu, J.; Lal, S. QSAR Models for Nitrogen Containing Monophosphonate and Bisphosphonate Derivatives as Human Farnesyl Pyrophosphate Synthase Inhibitors Based on Monte Carlo Method. *Drug Res.* **2019**, *69*, 159–167, <https://doi.org/10.1055/a-0652-5290>.
54. Tabti, K.; Sbai, A.; Maghat, H.; Lakhlifi, T.; Bouachrine, M. Computational exploration of the structural requirements of triazole derivatives as colchicine binding site inhibitors. *ChemistrySelect* **2023**, *8*, e202301707, <https://doi.org/10.1002/slct.202301707>.
55. Tropsha, A.; Gramatica, P.; Gombar, V.K. The importance of being earnest: validation is the absolute essential for successful application and interpretation of QSPR models. *QSAR Comb. Sci.* **2003**, *22*, 69–77, <https://doi.org/10.1002/qsar.200390007>.
56. Roy, K.; Mitra, I.; Kar, S.; Ojha, P.K.; Das, R.N.; Kabir, H. Comparative Studies on Some Metrics for External Validation of QSPR Models. *Journal of Chemical Information and Modeling American Chemical Society*: **2012**, *52*, 396–408, <https://doi.org/10.1021/ci200520g>.
57. Golbraikh, A.; Tropsha, A. Beware of q^2 !. *Journal of Molecular Graphics and Modelling* **2002**, *20*, 269–276, [https://doi.org/10.1016/S1093-3263\(01\)00123-1](https://doi.org/10.1016/S1093-3263(01)00123-1).
58. Zhang, D. A Coefficient of Determination for Generalized Linear Models. *Am. Stat.* **2017**, *71*, 310–316, <https://doi.org/10.1080/00031305.2016.1256839>.
59. Roy, K. On some aspects of validation of predictive quantitative structure–activity relationship models. *Expert Opin. Drug Discov.* **2007**, *2*, 1567–1577, <https://doi.org/10.1517/17460441.2.12.1567>.
60. Barber, C.; Heghes, C.; Johnston, L. A framework to support the application of the OECD guidance documents on (Q)SAR model validation and prediction assessment for regulatory decisions. *Comput. Toxicol.* **2024**, *30*, 100305, <https://doi.org/10.1016/j.comtox.2024.100305>.
61. Ouabane, M.; Tabti, K.; Hajji, H.; Elbouhi, M.; Khaldan, A.; Elkamel, K.; Sbai, A.; Aziz Ajana, M.; Sekkate, C.; Bouachrine, M.; Lakhlifi, T. Structure-odor relationship in pyrazines and derivatives: A physicochemical study using 3D-QSPR, HQSPR, Monte Carlo, molecular docking, ADME-Tox and molecular dynamics. *Arabian Journal of Chemistry* **2023**, *16*, 105207, <https://doi.org/10.1016/j.arabjc.2023.105207>.
62. Schneider, B.; Oliveira, R.A. de; Friedman, G.; Moraes, R.B. Association of biomarkers with successful ventilatory weaning in COVID-19 patients: an observational study. *Critical Care Science* **2024**, *36*, e20240158en, <https://doi.org/10.62675/2965-2774.20240158-en>.
63. Gramatica, P. Principles of QSAR models validation: internal and external. *QSAR & Combinatorial Science* **2007**, *26*, 694–701, <https://doi.org/10.1002/qsar.200610151>.
64. Trott, O.; Olson, A.J. AutoDock Vina: Improving the speed and accuracy of docking with a new scoring function, efficient optimization, and multithreading. *Journal of Computational Chemistry* **2010**, *31*, 455–461, <https://doi.org/10.1002/jcc.21334>.
65. Singh, N.; Singh, A.K. In Silico Structural Modeling and Binding Site Analysis of Cerebroside Sulfotransferase (CST): A Therapeutic Target for Developing Substrate Reduction Therapy for Metachromatic Leukodystrophy. *ACS Omega American Chemical Society* **2024**, *9*, 10748–10768, <https://doi.org/10.1021/acsomega.3c09462>.
66. Gilson, M.K.; Zhou, H.-X. Calculation of Protein-Ligand Binding Affinities. *Annual Review of Biophysics* **2007**, *36*, 21–42, <https://doi.org/10.1146/annurev.biophys.36.040306.132550>.
67. Aguilar-Carrillo, Y.; Soto-Urzuá, L.; Martínez-Martínez, M.D.L.Á.; Becerril-Ramírez, M.; Martínez-Morales, L.J. Computational Analysis of the Tripartite Interaction of Phasins (PhaP4 and 5)-Sigma Factor (σ_{24})-DNA of *Azospirillum brasilense* Sp7. *Polymers* **2024**, *16*, 611, <https://doi.org/10.3390/polym16050611>.

68. Zhang, Y.; Wang, Y.; Zhou, W.; Fan, Y.; Zhao, J.; Zhu, L.; Lu, S.; Lu, T.; Chen, Y.; Liu, H. A combined drug discovery strategy based on machine learning and molecular docking. *Chemical Biology & Drug Design* **2019**, *93*, 685-699, <https://doi.org/10.1111/cbdd.13494>.
69. Kramer, A.F.; Hahn, S.; Cohen, N.J.; Banich, M.T.; McAuley, E.; Harrison, C.R.; Chason, J.; Vakil, E.; Bardell, L.; Boileau, R.A. Ageing, fitness and neurocognitive function. *Nature* **1999**, *400*, 418-419, <https://doi.org/10.1038/22682>.
70. Tabti, K.; El Mchichi, L.; Moukhliiss, Y.; Singh, G.; Sbai, A. CoMFA Topomer, CoMFA, CoMSIA, HQSAR, docking molecular, dynamique study and ADMET study on phenyloxypropyl isoxazole derivatives for coxsackie virus B3 virus inhibitors activity. *Moroccan Journal of Chemistry* **2022**, *10*, 703-725, <https://doi.org/10.48317/IMIST.PRSM/morjchem-v10i4.34319>.
71. El Fadili, M.; Er-Rajy, M.; Kara, M.; Assouguem, A.; Belhassan, A.; Alotaibi, A.; Mrabti, N.N.; Fidan, H.; Ullah, R.; Ercisli, S. QSAR, ADMET in silico pharmacokinetics, molecular docking and molecular dynamics studies of novel bicyclo (aryl methyl) benzamides as potent GlyT1 inhibitors for the treatment of schizophrenia. *Pharmaceuticals* **2022**, *15*, 670, <https://doi.org/10.3390/ph15060670>.
72. Daina, A.; Michielin, O.; Zoete, V. SwissADME: a free web tool to evaluate pharmacokinetics, drug-likeness and medicinal chemistry friendliness of small molecules. *Scientific Reports* **2017**, *7*, 42717, <https://doi.org/10.1038/srep42717>.
73. Dulsat, J.; López-Nieto, B.; Estrada-Tejedor, R.; Borrell, J.I. Evaluation of Free Online ADMET Tools for Academic or Small Biotech Environments. *Molecules* **2023**, *28*, 776, <https://doi.org/10.3390/molecules28020776>.
74. Hubatsch, I.; Ragnarsson, E.G.E.; Artursson, P. Determination of drug permeability and prediction of drug absorption in Caco-2 monolayers. *Nature Protocols* **2007**, *2*, 2111-2119, <https://doi.org/10.1038/nprot.2007.303>.
75. Tabti, K.; Sbai, A.; Maghat, H.; Lakhlifi, T.; Bouachrine, M. Discovery of novel indoleamine 2, 3-dioxygenase-1 (IDO-1) inhibitors: pharmacophore-based 3D-QSAR, Gaussian field-based 3D-QSAR, docking, and binding free energy studies. *Structural Chemistry* **2023**, *35*, 135-160, <https://doi.org/10.1007/s11224-023-02213-0>.
76. Press, B.; Di Grandi, D. Permeability for Intestinal Absorption: Caco-2 Assay and Related Issues. *Current Drug Metabolism* **2008**, *9*, 893-900, <https://doi.org/10.2174/138920008786485119>.
77. Isa, A. S.; Uzairu, A.; Umar, U. M.; Ibrahim, M. T.; Umar, A. B.; Tabti, K.; Mukhtar, A. M. In silico exploration of novel EGFR-targeting compounds: integrative molecular modeling, docking, pharmacokinetics, and MD simulations for advancing anti-cervical cancer therapeutics. *Scientific Reports* **2025**, *15*, 7334, <https://doi.org/10.1038/s41598-025-91135-4>.
78. Suenderhauf, C.; Hammann, F.; Huwyler, J. Computational Prediction of Blood-Brain Barrier Permeability Using Decision Tree Induction. *Molecules* **2012**, *17*, 10429-10445, <https://doi.org/10.3390/molecules170910429>.
79. Zanger, U.M.; Schwab, M. Cytochrome P450 enzymes in drug metabolism: Regulation of gene expression, enzyme activities, and impact of genetic variation. *Pharmacology & Therapeutics* **2013**, *138*, 103-141, <https://doi.org/10.1016/j.pharmthera.2012.12.007>.

Publisher's Note & Disclaimer

The statements, opinions, and data presented in this publication are solely those of the individual author(s) and contributor(s) and do not necessarily reflect the views of the publisher and/or the editor(s). The publisher and/or the editor(s) disclaim any responsibility for the accuracy, completeness, or reliability of the content. Neither the publisher nor the editor(s) assume any legal liability for any errors, omissions, or consequences arising from the use of the information presented in this publication. Furthermore, the publisher and/or the editor(s) disclaim any liability for any injury, damage, or loss to persons or property that may result from the use of any ideas, methods, instructions, or products mentioned in the content. Readers are encouraged to independently verify any information before relying on it, and the publisher assumes no responsibility for any consequences arising from the use of materials contained in this publication.